VOLUME 9, NUMBER 10, OCTOBER 2009

NANO LETTERS

Letters

Nanoscale Mode Selector in Silicon Waveguide for on Chip Nanofocusing Applications

Boris Desiatov,† Ilya Goykhman,† and Uriel Levy*

Department of Applied Physics, The Benin School of Engineering and Computer Science, The Center for Nanoscience and Nanotechnology, The Hebrew University of Jerusalem, Jerusalem, 91904, Israel

Received April 7, 2009; Revised Manuscript Received August 11, 2009

ABSTRACT

We demonstrate a nanoscale mode selector supporting the propagation of the first antisymmetric mode of a silicon waveguide. The mode selector is based on embedding a short section of PhC into the waveguide. On the basis of the difference in *k*-vector distribution between orthogonal waveguide modes, the PhC can be designed to have a band gap for the fundamental mode, while allowing the transmission of the first antisymmetric mode. The device was tested by directly measuring the modal content before and after the PhC section using a near field scanning optical microscope. Extinction ratio was estimated to be ~23 dB. Finally, we provide numerical simulations demonstrating strong coupling of the antisymmetric mode to metallic nanotips. On the basis of the results, we believe that the mode selector may become an important building block in the realization of on chip nanofocusing devices.

The capability to tightly confine light beams is a cornerstone in the long quest for perusing miniaturization and integration of optical components at the nanoscale. A variety of techniques including, for example, near field scanning optical microscope,[1−3] metallic nanotapers[4−6] metamaterials,[7,8] plasmonic lenses,[9,10] and other subwavelength structures[11−15]

* Corresponding author, ulevy@cc.huji.ac.il.
† These authors contributed equally to this work.

10.1021/nl901110b CCC: $40.75
Published on Web 08/31/2009

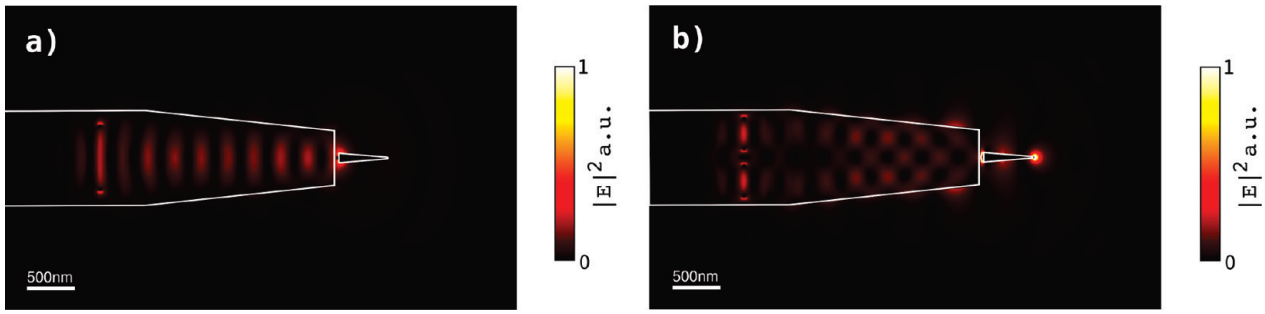

Figure 1. Calculated energy density distribution along the plane of symmetry in the vertical direction. The structure is excited by (a) symmetric waveguide mode and (b) antisymmetric waveguide mode. The excitation wavelength is 1.55 μm. The white lines represent the boundaries of the structure.

were exploited for tight focusing applications. Recent developments in photonics and plasmonics emphasize the fundamental importance of polarization in tight focusing scenarios. Of particular interest are systems exploiting radially polarized light beams, which are found to be beneficial in reducing the spot size at the focal plane under tight focusing illumination as well as in plasmonic focusing at the nanoscale.[16−19] While these demonstrations relied on the two-dimensional geometry of vector beams propagating in free space, there is a great advantage in confining light on-chip, using the planar geometry of modern integrated photonic circuits. Accordingly, one can think of the one-dimensional analogue of radial polarization, having an antisymmetric mode profile, in a similar way as the TE_1 waveguide mode is the one-dimensional (1D) equivalent of the TE_{01} mode in cylindrical coordinates. In analogy to two-dimensional tight focusing of radially polarized light, an antisymmetric mode is also expected to generate a strong longitudinal electric field component, which is needed for nanoscale light confinement and localization of an optical energy at the apex of nanotips.[4] An antisymmetric waveguide mode was recently employed for heat-assisted nanomagnetic recording applications providing an increase in magnetic disk drive storage density.[20]

Nanotips and nanotapers can be excited by variety of techniques, yet the excitation efficiency relies on proper selection of the modal structure that is coupled into the tip. Figure 1 shows a comparison of the energy density at the apex of a metallic tip that is excited by the fundamental and the first antisymmetric waveguide modes. The results were calculated by three-dimensional finite difference time domain (FDTD) simulation using a grid of 5 nm and excitation wavelength of 1.55 μm. The simulated structure consists of a 250 nm thick silicon waveguide (refractive index of 3.46) that is tapered from 1 to 0.6 μm width over a length of 2 μm and butt coupled to a 250 nm thick silver nanotip having a base width of 100 nm and length of 500 nm. The Ag permittivity is modeled by a Drude model including damping.[21] For the simulated realistic structure, we assumed a rounded tip apex having a radius of 15 nm. The gap between the waveguide and the tip is 20 nm. We found this gap helpful in enhancing the energy density at the apex of the tip. The structure is surrounded by a symmetric oxide cladding (refractive index of 1.46).

The simulation results clearly show a significant enhancement of the energy density at the apex of the tip for the case of excitation by the antisymmetric waveguide mode compared with the case of symmetric mode excitation. We found the ratio of energy density between these two cases to be $\sim$100 (we believe that this ratio can be further enhanced by detailed optimization of the structure). For this reason, the goal of this work is to generate and isolate the antisymmetric mode on chip.

Previous approaches for the obtaining of the antisymmetric waveguide mode are based on the employment of adiabatic (for example multimode interference devices)[22−24] or nonadiabatic mode converters.[25] Such devices are capable of converting a known mode (e.g., the fundamental mode) to the desired one (e.g., an antisymmetric mode). However, the adiabatic conversion is typically achieved over a relatively long distance (ranging from tens of micrometers to few centimeters), while the nonadiabatic solutions are often very sensitive to variations of input signal, strongly affected by fabrication imperfections, and may suffer from low modal purity.

In this paper we take a different approach for obtaining a "pure" antisymmetric mode by realizing a mode-selective type device. The original role of the mode selector is to support a specific (known) modal pattern, while "blocking" all other modes from propagating through the device. Recently, it was theoretically suggested that the field profile propagating in ridge waveguide can be controlled by embedding a periodic structure into the waveguide core.[26]

For our purpose of supporting the propagation of a second (antisymmetric) mode only we adopted this approach by embedding a short section of two-dimensional photonic crystal (PhC) in a multimode silicon waveguide, as illustrated in Figure 2. In this hybrid waveguide-PhC structure the guiding mechanism is still governed by total internal reflection (TIR), but at the same time the propagating light should also satisfy the dispersion relation of the PhC. Therefore, it is possible to control the modal pattern of light propagating in the waveguide using different band diagram designs. In particular, taking an advantage of the dispersion properties of the PhC, one can "engineer" a device with multiple nodal points in the lowest-order mode (i.e., the lowest-order mode is different from the fundamental mode).

The operation principle of the mode selector is easily understood by using plane wave decomposition, based on

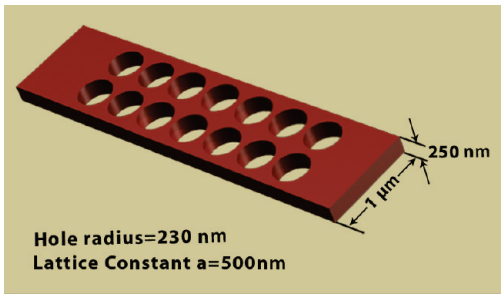

Figure 2. Schematic illustration of the mode selector.

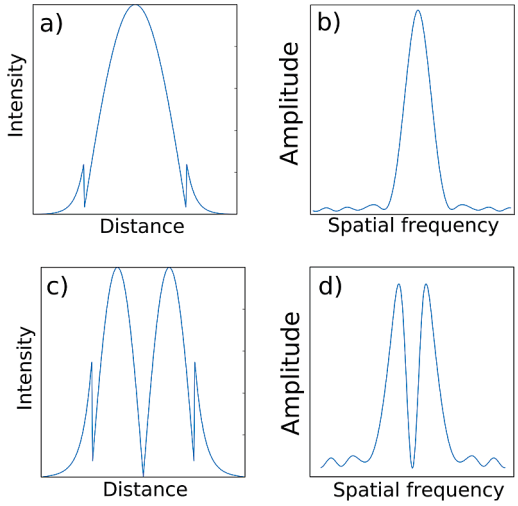

Figure 3. (a) Mode profile and (b) Fourier transform of the symmetric mode. (c and d) The same for the antisymmetric mode.

the difference in k-vector distribution for the first two modes. By taking a spatial Fourier transform of each mode profile along the transverse y-direction, one can notice that most of the energy of the fundamental mode is carried by plane waves with k-vector nearly parallel to the propagation x-direction. This is in contrast to the antisymmetric mode, where most of its energy is carried by k-vectors which are tilted with respect to propagation axis (see Figure 3). Therefore, for a given operational frequency we designed the band structure of the PhC core to have a band gap for parallel k-vector, while supporting the propagation of the tilted k-vectors in such way that the propagation of the fundamental mode is no longer allowed. This concept is depicted in the isofrequency diagram of the two-dimensional (2D) square lattice photonic crystal, consisting of air holes truncated into silicon slab suspended in air. According to Figure 4, for input wavelength of 1.55 μm which is equivalent to a normalized frequency of $0.32(c/a)$, where c is the speed of light and a is the period of the PhC, the propagation of the fundamental mode ($k_x = \beta$, $k_y = 0$) through the PhC is forbidden because of the bang gap appearing in the x-direction (red dot). On the basis of the isofrequency diagram, the minimal transverse component of a wave vector at the same frequency is $k_y(\text{min}) = 0.3(2\pi/a)$, marked by the blue dot. Taking into account the TIR condition, the minimum number of nodes in the field pattern can be calculated by $m \approx k_y(\text{min})\cdot d/\pi = 0.6d/a$, where d is the waveguide width. Consequently, a selection of

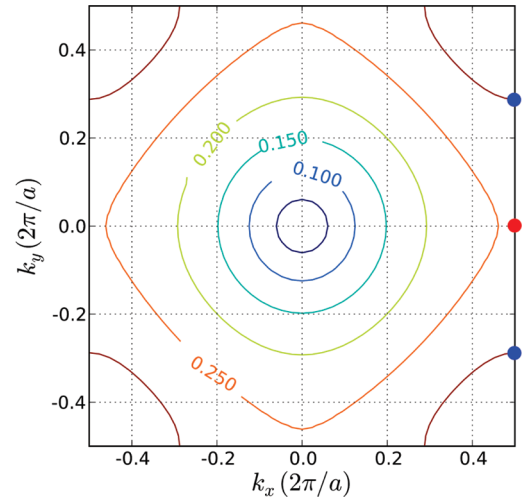

Figure 4. Isofrequency diagram showing the first band of the PhC.

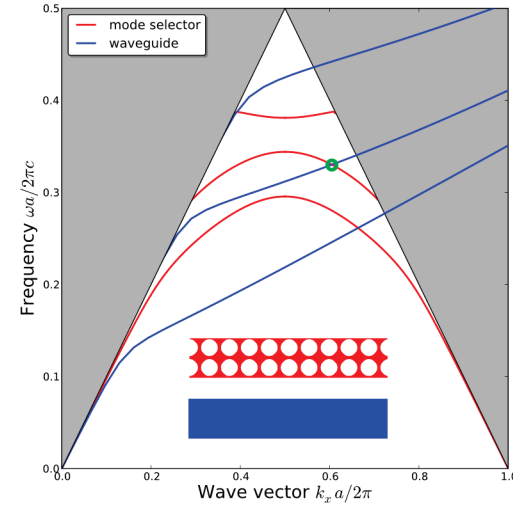

Figure 5. Numerically calculated band structure of the mode selector (red lines) superimposed onto the dispersion curve of the input waveguide (blue lines). The green circle indicates the intersection between the second waveguide mode and the second mode of the mode selector, which occurs at a wavelength of 1541 nm. The gray area represents the light cone.

specific mode profile originates from a pure dimensional relation between the waveguide and the PhC lattice constant. For this reason, to obtain a lowest order mode with $m = 2$ (antisymmetric profile), we choose a waveguide width to be twice that of the PhC period ($d = 1$ μm, $a = 0.5$ μm).

One can gain further understanding of the working principle of the mode selector by calculating the band structure of the mode selector and superimpose it on the dispersion curve of the input ridge waveguide as shown in Figure 5. The green circle marks the intersection between the second waveguide mode and the second mode of the PhC. The intersection occurs at a wavelength of 1541 nm, very close to our operating wavelength. In contrast, the first waveguide mode does not intersect any of the PhC modes around our wavelength of operation.

To verify our expectation, we performed a three dimensional (3D) FDTD simulation. The results are shown in

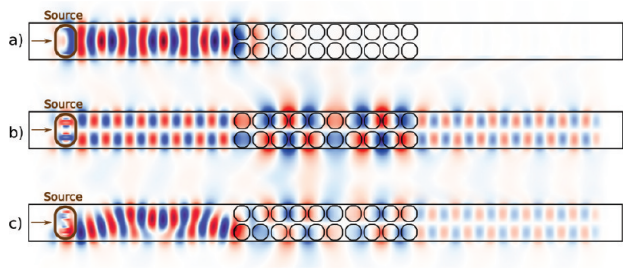

Figure 6. 3D FDTD numerical simulation of mode selector for different input modal contents: (a) first waveguide mode, (b) second waveguide mode, and (c) superposition of first and second modes.

Figure 6. A continuous TE (in-plane) polarized signal comprising 50% fundamental and 50% antisymmetric mode was launched into the mode selector. At the steady state frequency of 0.32(c/a) the field at the output of the device has an odd modal profile, while the field with even symmetry is reflected and is not allowed to propagate through the PhC section. According to the simulation the antisymmetric mode passes the device with some attenuation due to mode mismatch between the strip and the PhC waveguides. For our device length (5 μm) the expected transmission efficiency is ~80%. To minimize the device loss, one can use an adiabatic tapered interface between the silicon waveguide and the PhC structure, allowing an adiabatic transition between the waveguide and PhC Bloch modes.

Our mode-selector was fabricated using silicon-on-insulator substrate with device layer of 250 nm on top of 3 μm buried oxide (BOX). Both the waveguide and the PhC were defined with standard electron-beam lithography followed by inductively coupled plasma (ICP) reactive ion etching (RIE). A 5 μm long PhC segment with a period of 500 nm and hole radius of 210 nm was "drilled" into a 1 μm wide multimode silicon waveguide, resulting in a minimal feature separation of 40 nm (Figure 7). To avoid leakage of light into substrate modes, a membrane ("air-bridge") configuration was realized by additional lithographic step and isotropic wet etching of the BOX with buffered hydrofluoric acid (BHF). Such air bridge structures are now commonly used and were recently utilized for the demonstration of 1D PhC cavities with high quality factors and ultrasmall modal volumes.[27] To ensure high coupling efficiency between the waveguide and the incoming fiber, an adiabatic taper was fabricated at the end of the waveguide.

A major challenge in the characterization of multimode optical device is the difficulty to control the mode combination within a nanophotonic structure. The relative modal content in the multimode waveguide is greatly affected by the coupling conditions (fiber position, facet quality, etc.). In practice, the most reasonable approach allowing to experimentally verify the modal structure of the multimode waveguide before the mode selector section is probably the near-field technique. As a result, following the fabrication process our mode selector was tested by near-field scanning optical microscopy (NSOM). Conducting the near-field characterization we have acquired in situ qualitative and quantitative information about intensity distribution, extinction ratio, and wavelength sensitivity of a mode-selector under test. The NSOM was recently used to characterize light propagation in silicon waveguides and PhC structures.[28−31]

Throughout all NSOM measurements we used a 70 mW continuous wave optical signal from a diode laser at fixed wavelength of $\lambda_0 = 1552.12$ nm. Light was launched into the silicon waveguide (taper width of ~2 μm) via a lensed fiber (~2.5 μm spot size) using butt coupling configuration, while obtaining an optimum alignment according to maximum transmission feedback from the output InGaAs detector. NSOM tips with aperture size of 300 nm were used to measure the spatial intensity profile slightly before and after the mode-selector section, as presented in Figure 8. On the basis of the NSOM measurement results, the input signal (Figure 8a,b) is ascribed to superposition of the first and second modes as evident by the "snakelike" pattern shown in the measured intensity distribution. The snakelike pattern is the result of beating between two modes due to a difference in their effective refractive indices. On the other hand, the NSOM results at the exit of the device (Figure 8d,e) clearly show a null at the center of the waveguide along the propagation direction, indicating that at the output of the mode selector most of the energy is carried by the antisymmetric mode.

To quantify these observations, we have simulated the intensity distribution resulting from various possible combinations of the first two modes in the form of $I = |E|^2 = |aE_1 + (1 - a)E_2|^2$, where a denotes a weight factor and E_1 and E_2 are the electric fields of the first and the second mode with effective indexes of $n_1 = 2.7972$ and $n_2 = 2.4615$, respectively. In addition, to guarantee a better correlation between the computer calculations and the expected NSOM

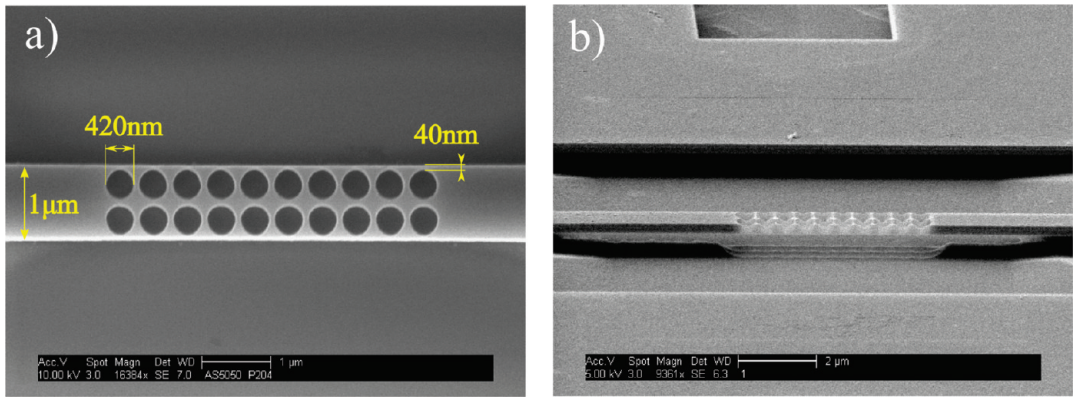

Figure 7. Scanning electron micrograph of the mode selector: (a) top view and (b) slanted view showing the air bridge configuration.

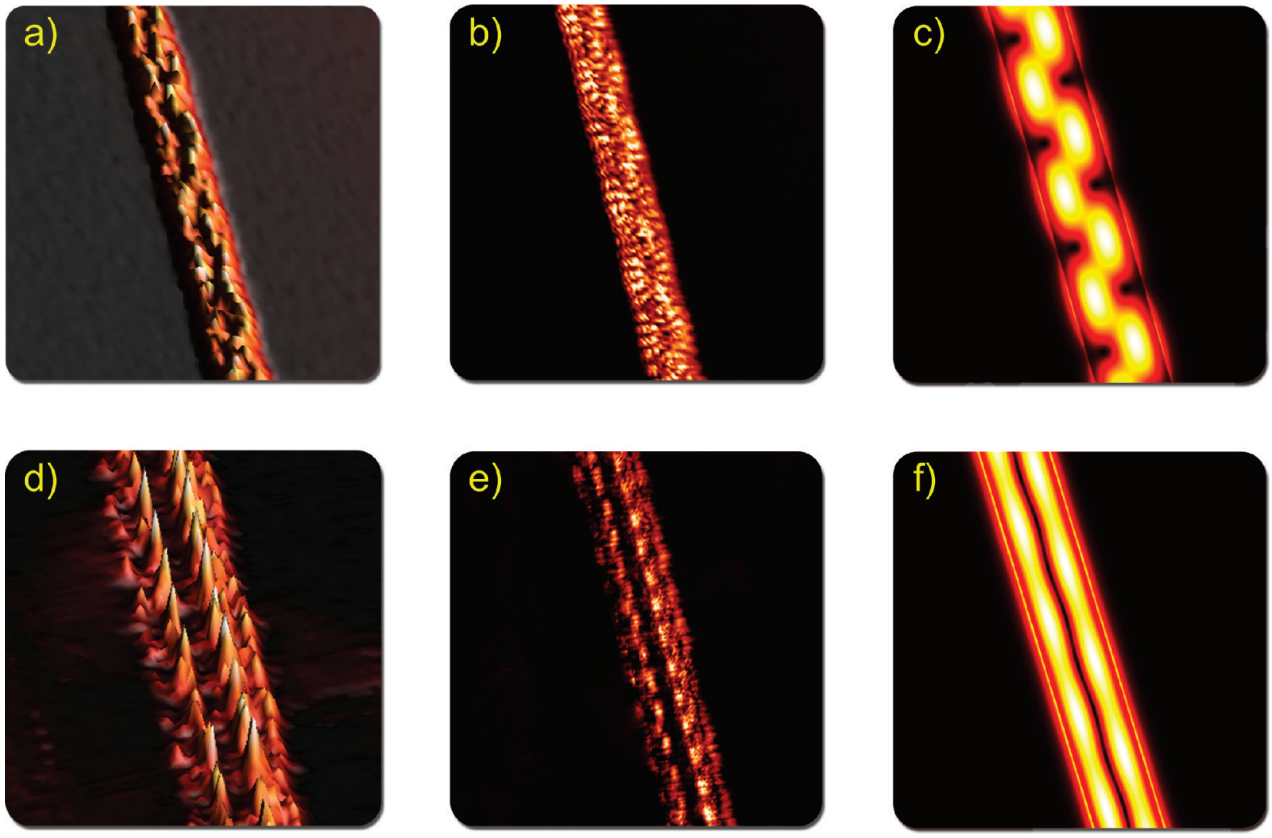

Figure 8. NSOM measurement results. (a, b) Measured intensity at the input waveguide (3D and 2D representations respectively). (c) Simulated intensity at the input waveguide. (d, e) Measured intensity at the output of device (3D and 2D representations, respectively). (f) Simulated intensity at the output of device.

results, we convolved the simulated field profile with the 300 nm NSOM tip aperture. By fitting the simulation results to the NSOM measurements (after averaging the measured intensity along the propagation axis of the waveguide), we estimate that the electric field at the input of the mode selector is composed of 60% first mode and 40% second mode, whereas the field distribution at the output is close to 10% first and 90% second mode. The fitting accuracy was estimated to be ~5%. To appraise mode selection properties we defined the extinction ratio of the device as the ratio between the power attenuation of the two modes according to $ER = 10 \log\{[P_2/P_1]_{out}/[P_2/P_1]_{in}\}$. This value was found to be 23 ± 7 dB. The loss of our device is defined as loss $= -10 \log(P_{2,out}/P_{2,in})$. This value was found to be 3 ± 1.5 dB. This value is higher than the expected insertion loss (~1 dB, corresponding to 80% transmission). The difference is primarily attributed to the nonperfect fabrication process (e.g., roughness, nonuniformity of the hole dimensions, and shift from their expected position). We believe that this result can be improved by carefully optimizing the fabrication process. In addition, the loss can be further reduced by optimizing the interface between the ridge waveguide and the PhC structure, e.g., by using an adiabatic transition between the two structures.

In conclusion, we designed, fabricated, and experimentally demonstrated a mode selector supporting the propagation of the first antisymmetric mode of a silicon waveguide. The mode selector is based on embedding a short section of PhC into the waveguide. On the basis of the difference in *k*-vector distribution between orthogonal waveguide modes, the PhC can be designed to have a band gap for the fundamental mode, while allowing the transmission of the first antisymmetric mode. The device was tested by directly measuring the modal content before and after the PhC section using a near field scanning optical microscope. The measured extinction ratio was estimated to be ~23 dB and the loss is about 3 dB.

References

(1) Ash, E. A.; Nicholls, G. Super-Resolution Aperture Scanning Microscope. *Nature (London)* **1972**, *237*, 510–512.
(2) Lewis, A.; Isaacson, M.; Harootunian, A.; Muray, A. Development of a 500 Å spatial resolution light microscope I. Light is efficiently transmitted through λ/16 diameter apertures. *Ultramicroscopy* **1984**, *13*, 227–232. [http://dx.doi.org/10.1016/0304-3991(84)90201-8].
(3) Pohl, D. W.; Denk, W.; Lanz, M. Optical stethoscopy: image recording with resolution λ/20. *Appl. Phys. Lett.* **1984**, *44*, 651–653. [http://link.aip.org/link/?APPLAB/44/651/1].
(4) Stockman, M. I. Nanofocusing of optical energy in tapered plasmonic waveguides. *Phys. Rev. Lett.* **2004**, *93*, 137404−1-4.. [http://prola.aps.org/abstract/PRL/v93/i13/e137404].
(5) Verhagen, E; Polman, A; Kuipers, L. K. Nanofocusing in laterally tapered plasmonic waveguides. *Opt. Express* **2008**, *16*, 45–57. [http://www.opticsinfobase.org/abstract.cfm?URI=oe-16-1-45].
(6) Ropers, C.; Neacsu, C. C.; Elsaesser, T.; Albrecht, M.; Raschke, M. B.; Lienau, C. Grating-coupling of surface plasmons onto metallic tips: a nanoconfined light source. *Nano Lett.* **2007**, *7*, 2784–2788. [http://pubs.acs.org/doi/abs/10.1021/nl071340m].
(7) Pendry, J. B. Negative refraction makes a perfect lens. *Phys. Rev. Lett.* **2000**, *85*, 3966–3969. [http://link.aps.org/doi/10.1103/PhysRevLett.85.3966].
(8) Valentine, J.; Zhang, S.; Zentgraf, T.; Ulin-Avila, E.; Genov, D. A.; Bartal, G.; Zhang, X. Three-dimensional optical metamaterial with a

negative refractive index. *Nature* **2008**, *455*, 376–379. [http://www.nature.com/nature/journal/v455/n7211/suppinfo/nature07247_S1.html].
(9) Liu, Z.; Steele, J. M.; Srituravanich, W.; Pikus, Y.; Sun, C.; Zhang, X. Focusing surface plasmons with plasmonic lens. *Nano Lett.* **2005**, *5*, 1726–1729. [http://pubs.acs.org/doi/abs/10.1021/nl051013j].
(10) Fang, N.; Lee, H.; Sun, C.; Zhang, X. Sub-Diffraction-Limited Optical Imaging with a Silver Superlens. *Science* **2005**, *308*, 534–537. [http://dx.doi.org/10.1126/science.1108759].
(11) Levy, U.; Nezhad, M.; Kim, H.-C.; Tsai, C.-H.; Pang, L.; Fainman, Y. Implementation of a graded-index medium by use of subwavelength structures with graded fill factor. *J. Opt. Soc. Am. A* **2005**, *22*, 724–733. [http://www.opticsinfobase.org/abstract.cfm?URI=josaa-22−4-724].
(12) Levy, U.; Abashin, M.; Ikeda, K.; Krishnamoorthy, A.; Cunningham, J.; Fainman, Y. Inhomogeneous Dielectric Metamaterials with Space-Variant Polarizability. *Phy. Rev. Lett,* **2007**, *98*, 243901–243904. [http://link.aps.org/doi/10.1103/PhysRevLett.98.243901].
(13) Matsumoto, T.; Eom, K.-S.; Baba, T. Focusing of light by negative refraction in a photonic crystal slab superlens on silicon-on-insulator substrate. *Opt. Lett.* **2006**, *31*, 2786–2788. [http://www.opticsinfobase.org/abstract.cfm?URI=ol-31−18−2786].
(14) Fabre, N.; Lalouat, L.; Cluzel, B.; Melique, X.; Lippens, D.; Fornel, F.; Vanbesien, O. Optical Near-Field Microscopy of Light Focusing through a Photonic Crystal Flat Lens. *Phys. Rev. Lett.* **2008**, *101*, 073901[http://link.aps.org/doi/10.1103/PhysRevLett.101.073901].
(15) Schonbrun, E.; Wu, Q.; Park, W.; Yamashita, T.; Summers, C. J.; Abashin, M.; Fainman, Y. Wave front evolution of negatively refracted waves in a photonic crystal. *Appl. Phys. Lett.* **2007**, *90*, 41113−1-3. [http://dx.doi.org/10.1063/1.2435344].
(16) Dorn, R.; Quabis, S.; Leuchs, G. Sharper focus for a radially polarized light beam. *Phys. Rev. Lett.* **2003**, *91*, 233901. [http://prola.aps.org/abstract/PRL/v91/i23/e233901].
(17) Zhan, Q. Cylindrical vector beams: from mathematical concepts to applications. *Adv. Opt. Photon.* **2009**, *1*, 1–57. [http://www.opticsinfobase.org/aop/abstract.cfm?URI=aop-1-1-1].
(18) Lerman, G. M.; Levy, U. Effect of radial polarization and apodization on spot size under tight focusing conditions. *Opt. Express* **2008**, *16*, 4567–4581. [http://www.opticsinfobase.org/abstract.cfm?uri=oe-16−7-4567].
(19) Yanai, A.; Levy, U. Plasmonic focusing with a coaxial structure illuminated by radially polarized light. *Opt. Express* **2009**, *17*, 924–932. [http://www.opticsinfobase.org/oe/abstract.cfm?URI=oe-17−2-924].
(20) Challener, W. A.; Peng, C; Itagi, A. V.; Karns, D.; Peng, W.; Peng, Y.; Yang, X.; Zhu, X.; Gokemeijer, N. J.; Hsia, Y.-T.; Ju, G.; Rottmayer, R. E.; Seigler, M. A.; Gage, E. C. Heat-assisted magnetic recording by a near-field transducer with efficient optical energy transfer. *Nature Photon.* **2009**, *3*, 220–224. [http://www.nature.com/nphoton/journal/v3/n4/abs/nphoton.2009.26.html].
(21) Johnson, P. B.; Christy, R. W. Optical Constants of the Noble Metals. *Phys. Rev. B* **1972**, *6*, 4370–4379.
(22) Lee, B.-T.; Shin, S.-Y. Mode-order converter in a multimode waveguide. *Opt. Lett.* **2003**, *28*, 1660–1662. [http://www.opticsinfobase.org/ol/abstract.cfm?URI=ol-28-18-1660].
(23) Park, J. B.; Yeo, D.-M.; Shin, S.-Y. Variable optical mode generator in a multimode waveguide. *IEEE Photonics Technol. Lett.* **2006**, *18* (20), 2084–2086. [http://dx.doi.org/10.1109/LPT.2006.883203].
(24) Huang, Y.; Xu, G.; Ho, S.-T. An Ultracompact Optical Mode Order Converter. *IEEE Photonics Technol. Lett.* **2006**, *18* (21), 2281–2283. [http://ieeexplore.ieee.org/stamp/stamp.jsp?arnumber=1715401&isnumber=36041].
(25) Yang, M.; Chen, H.; Webb, K. J.; Minin, S.; Chuang, S. L.; Cueva, G. R. Demonstration of mode conversion in an irregular waveguide. *Opt. Lett.* **2006**, *31*, 383–385. [http://www.opticsinfobase.org/ol/abstract.cfm?URI=ol-31-3-383].
(26) Yu, X.; Lau, W. T.; Fan, S. Anomalous modal structure in a waveguide with a photonic crystal core. *Opt. Lett.* **2006**, *31*, 742–744. [http://www.opticsinfobase.org/ol/abstract.cfm?URI=ol-31-6-742].
(27) Deotare, P. B.; McCutcheon, M. W.; Frank, I. W.; Khan, M.; Loněar, M. High quality factor photonic crystal nanobeam cavities. *Appl. Phys. Lett.* **2009**, *94*, 121106. [http://link.aip.org/link/?APPLAB/94/121106/1].
(28) Bozhevolnyi, S.; Kuipers, L. TOPICAL REVIEW: Near-field characterization of photonic crystal waveguides. *Semicond. Sci. Technol.* **2006**, *21* (5), R1–R16. [http://dx.doi.org/10.1088/0268−1242/21/5/R01].
(29) Gersen, H.; Karle, T. J.; Engelen, R. J. P.; Bogaerts, W.; Korterik, J. P.; Hulst van, N. F.; Krauss, T. F.; Kuipers, L. Direct Observation of Bloch Harmonics and Negative Phase Velocity in Photonic Crystal Waveguides. *Phys. Rev. Lett.* **2005**, *94* (12), 123901–1. [http://link.aps.org/doi/10.1103/PhysRevLett.94.123901].
(30) Abashin, M.; Tortora, P.; Märki, I; Levy, U.; Nakagawa, W.; Vaccaro, L.; Herzig, H. P.; Fainman, Y. Near-field characterization of propagating optical modes in photonic crystal waveguides. *Opt. Express* **2006**, *14* (4)), 1643–1657. [http://www.opticsinfobase.org/abstract.cfm?URI=oe-14-4-1643].
(31) Tortora, P.; Abashin, M.; Märki, I.; Nakagawa, W.; Vaccaro, L.; Salt, M.; Herzig, H. P.; Levy, U.; Fainman, S. Observation of amplitude and phase in ridge and photonic crystal waveguides operating at 1.55 μm using heterodyne scanning near-field optical microscopy. *Opt. Lett.* **2005**, *30* (21), 2885. [http://www.opticsinfobase.org/ol/abstract.cfm?URI=ol-30-21-2885].

NL901110B